High efficiency molecular-beam ionization detector with short ionization region

K. Kuhnke and K. Kern
Institut de Physique Expérimentale, EPFL, CH-1015 Lausanne, Switzerland

R. David and G. Comsa
Institut für Grenzflächenforschung und Vakuumphysik, KFA-Forschungszentrum Jülich, D-52425 Jülich, Germany

(Received 23 June 1994; accepted for publication 8 August 1994)

A mass selective electron-impact ionization detector for use in energy resolved thermal He scattering experiments is presented. The detector combines a short effective ionization region (approximately 3 mm FWHM) with a high detection efficiency of 10^{-5} at 2 mA electron emission. An efficiency of 10^{-4} at 10 mA emission current can be achieved if time resolution below 20 μs is dispensable. The design is discussed and measurements of detection efficiency and time resolution are presented. The ionizer can likewise be employed for an efficient detection of other types of atoms or molecules.

I. INTRODUCTION

He detectors find an important application in vacuum science (leak testing) and, more specialized, as detectors in He surface scattering devices. Although a number of different mechanisms can be utilized to detect He atoms,[1] only the electron-impact ionization detector[2] combines reasonable efficiency, simplicity of design, and a detection time resolution in the lower microsecond range for thermal energy atoms (i.e., at kinetic energies between 10 and 100 meV).

This type of detector is commercially available for rest gas analysis in a multitude of models. However, these are generally not optimized for both efficiency and time resolution. A fairly good compromise with respect to this problem were ionizers like the model 041-1 from the former Extranuclear Laboratories, Inc., which have a geometry similar to the one in Ref. 3 and an effective ionization length of about 5 mm.[4] However, this device can detect only about one atom in a million in a thermal He beam. This probability is far from the theoretical limits at an electron emission current of 5 mA. There is obviously still opportunity to achieve a higher efficiency and also a shorter ionization length. The demand for this development is primarily triggered by inelastic He surface scattering where an increased efficiency will either reduce the measuring time (typically in the range of 1 min–1 h for energy resolved measurements) or will allow improvement of both angular and energy resolution.

Inelastic thermal energy He scattering is a method which allows the study of surface phonons of solid samples with high-energy resolution.[5] The necessity for a good time resolution and a short length of the ionization volume of the detector arises from the fact that in these experiments the energy analysis of the scattered atoms is most commonly accomplished by the time-of-flight (TOF) method, where the thermal energy He beam is chopped mechanically, and these short pulses disperse on their flight path to the detector. The longer the intersection of flight path and ionization volume, the larger the uncertainty in the length of the individual flight path for a detected atom. This uncertainty reduces the energy resolution of the experiment. For a typical beam energy of 18 meV and a flight path of 1 m, the ionization region (INR) of the detector must be shorter than 5.5 mm in order to allow a detector energy resolution of better than 0.2 meV. The total energy resolution in machines presently used is typically 0.5 meV.[6] Increasing the time resolution requires a shortening of the length of the INR, which in consequence reduces the detector efficiency, because the electron charge density in the INR cannot be increased arbitrarily (see Sec. II). The length of the INR is the most important contribution to the detector time resolution for thermal energy beams. Other contributions are the distribution of ion flight times between ionization and ion detection and the jitter in the electronics (including the jitter in pulse formation and in channeltron rise time). These two factors are negligible in the example given above (beam energy 18 meV, energy resolution 0.2 meV) as the required time resolution is only 6 μs.

In this paper we present the design of an ionization detector with high performance for energy resolved He surface scattering. Based on ion-optical arguments we will show how the efficiency for ionization and the transmission through the quadrupole mass analyzer (QMA) can be increased by the ionizer design. The ionizer presented here has, in addition to a very short ionization region ($\approx$3 mm FWHM), an ionization efficiency of 10^{-4} for thermal He atoms at 10 mA electron emission.

The paper is organized as follows: In Sec. II we discuss the operation principles of the ionization detector and focus on the aspects which are important for improved performance. The ionizer design is presented and described in Sec. III A, while two designs for background reduction are discussed in Sec. III B. In Sec. IV we present measurements of efficiency and time resolution, the two important properties of the ionizer, and conclude with a summary in Sec. V.

II. ELECTRON-IMPACT IONIZATION AND MASS SELECTION

Figure 1 shows the successive stages in the detection of a thermal energy neutral particle beam. The atom enters the detector from the left and drifts through a volume surrounded

 0034-6748/94/65(11)/3458/8/$6.00

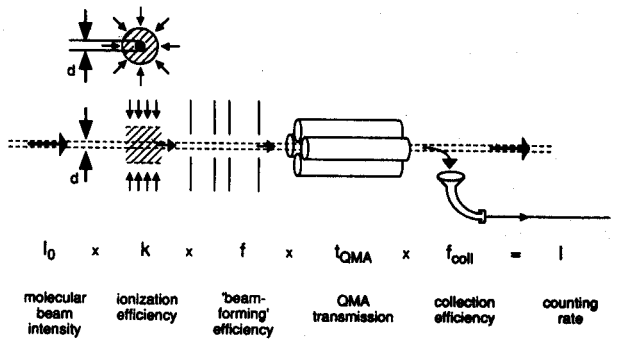

FIG. 1. Schematic of an electron bombardment ionization detector with mass selection by a QMA. Below the scheme the factors that determine the counting rate I are introduced. For the ionization region INR (shaded area) we show a side view and, above, the cross section. The molecular beam of diameter d which passes freely through the device is indicated by the two dashed lines and two large arrows. The electrons radially traverse the beam as symbolized by the small arrows outside the INR. The small arrows within the molecular beam symbolize the ion paths.

by a cylindrical grid. An electron beam is accelerated towards the grid, traverses the molecular beam and thus defines the INR in which ions are created. After extraction from this region the ions are injected into a mass selective device, either a magnetic sector analyzer or a QMA. We use the latter, because it has a variable mass resolution and the ion transmission is almost independent of the ion velocity over a wide range. The mass selected ions leave the QMA and are accelerated towards the channeltron entrance at a potential of -2.5 kV. Practically every ion reaching the channeltron creates an electrical pulse, which is amplified and transformed into a standard pulse for further processing.

In the following we discuss quantitatively aspects of the He ionization with regard to the properties of the QMA.

In the INR, the electrons emitted by a hot filament are accelerated towards the grid, traverse the thermal energy atom beam, and ionize atoms with a probability determined by the cross section for electron-impact ionization (which is a function of the electron energy). Assuming that the charge density is sufficiently low and the ionization efficiency is much smaller than unity everywhere in the INR, the integral ionization efficiency for a cylindrical geometry, in which all electrons pass *through the axis* of the molecular beam, is given by

$$k=\frac{I_{He^+}}{I_{He}}=\frac{4}{\pi}\frac{\sigma_{ion}\eta}{d}\left\langle\frac{1}{v}\right\rangle I_{e^-}. \quad (1)$$

Here, k is the ratio between the number of created ions I_{He^+} and the number of incoming thermal atoms I_{He} (see also Fig. 1), σ_{ion} the ionization cross section of a He atom for electron bombardment at the given electron energy, and d the diameter of the thermal beam in the INR.[7] η is the mean number of INR crossings for an emitted electron, $\langle 1/v\rangle$ the mean reciprocal velocity in the thermal beam, and I_{e^-} the filament electron emission in electrons per time unit (particle current).[8] With $\sigma_{ion}=3.5\times10^{-21}$ m^2 (at its maximum at $E=110$ eV),[9] a beam diameter of $d=1$ mm, $\eta=3$ (see Sec. IV A), the mean value of the reciprocal velocity in the flux of an effusive He beam at 300 K $\langle 1/v\rangle=(1260\ \text{m/s})^{-1}$, and an electron emission of 1.25×10^{16} s^{-1} (charge current: 2 mA), the theoretical efficiency limit is thus 1.3×10^{-4}.

We note here that although Eq. (1) has been derived for a strictly radial electron beam, the calculation for the opposite extreme, a homogeneous electron distribution in the INR, yields the same formula except a factor of 1 instead of the prefactor $4/\pi$. We also note that the length of the INR does not appear explicitly in Eq. (1). However, the INR cannot be made arbitrarily short, because of charge-density effects that will be discussed in the next two paragraphs.

An ion created by electron impact suddenly experiences the electric field due to the electron charge distribution and due to the fields from adjacent electrodes. The positive ion sees a potential well with a minimum on the INR axis. For an emission current of 2 mA, an INR length of 3 mm, and a cage diameter of 8 mm, the potential minimum is approximately 24 V more negative than the grid potential (see Appendix). Ions created within a cylinder of 4 mm in diameter around the axis of the INR originate from potentials that differ by more than 6 V and thus give rise to a corresponding distribution of kinetic energies in the ion beam. The consequence is a spreading of the flight times on the path between ionizer and channeltron, resulting in a contribution to the time resolution of the detector. The contributions to the velocity spread that arise from the thermal velocity of the parent atom and from the momentum transfer by the ionizing electron are both negligible ($E_{kin}<0.1$ eV just after the ionization). These contributions do not have to be taken into account even for ion trajectories *within* the INR. For counting rates that are typical for He scattering devices ($<10^6$ s^{-1}), the ion charge density can always be neglected.

Also in the direction along the INR axis a potential well can result from the electron charge density so that ions that are created inside the well might be trapped. The potential of the extracting electrodes must thus be low enough to avoid the formation of such a pit. The possible trapping of ions and the increasing width in the ion velocity distribution are the main reasons why the charge density in the INR should not exceed a certain limit.

The extracted ions pass through a lens system and are subsequently injected into a QMA. In order to achieve a proper mass separation the He ions must spend a certain number of cycles in the high-frequency quadrupole field. Thus the maximum kinetic energy of the ions shall not exceed a certain limit. In order to well separate the He ions from the H_2 background, this limit is 60 eV[10] when a QMA with a length of 210 mm and a resonance frequency of 4.5 MHz[11] is employed. The injection of ions into the QMA has to occur close to the QMA axis. The ions will pass through the QMA on stable trajectories if the ion-beam diameter and its divergence are small enough. In the four-dimensional phase space, in which the space and velocity coordinates *along* the beam axis are not taken into account, the volume of transmittance on stable trajectories is represented by an ellipsoid. The shape of the ellipsoid depends on the phase of the high-frequency field at the instance when the ion enters the QMA. Stable trajectories can be obtained for all phases when the divergence for a beam focused onto the QMA entrance is smaller than a certain value which depends on ion

velocity, QMA dimensions, and mass resolution.[12] For a 60 eV He^+ beam and an effective QMA electrode distance of $2R_0=16.7$ mm, the maximum accepted angle with respect to the axis is 12°. For the same parameters the maximum accepted beam diameter for a perfectly collimated beam is 3 mm. With increasing deviation from perfect collimation the accepted beam diameter is continuously reduced; it vanishes when the angle of divergence becomes 12°. The conditions imposed on the ion beam when injected into the QMA are thus rather strict. We will take these aspects into account when discussing the ionizer design in the next section.

An important improvement of the performance of the complete detector assembly can be achieved by enhancing the capture of the ions that exit the QMA. The solution of the equations of motion for the ions within the mass filter[12] leads to the conclusion that the distribution of the ions leaving the filter is by far broader in (six-dimensional) phase space than the distribution of the injected ions. This is due to the fact that the ion energy is not conserved in the presence of the strong oscillating electric field. We estimate that ions leaving the QMA may possess energies up to several hundred electron volts.[13] The lower energy ions may exit with an angle of 45° or more with respect to the QMA axis.[14] We conclude that the ion collection efficiency f_{coll} (see Fig. 1) is probably much smaller than 1 and we guess that this is the most significant residual loss of ions in the detection process. In order to detect as many ions as possible, we developed a deflector plate (described in Sec. III B), which also pushes those ions into the channeltron which follow more extreme trajectories.

III. DETECTOR DESIGN

A. Ionizer design

In the previous section we saw that an estimate for the theoretical ionization efficiency at 2 mA emission is 1.3×10^{-4}. However, the commercial detector achieves a total counting efficiency of only about 10^{-6} at 5 mA emission (see Sec. IV B). It can be concluded that either the number of created ions is smaller than it could be or a significant part of the created ions is lost on the way to the channeltron. In this section we will show that both can happen, and we will discuss means to increase the efficiency.

First, in the commercial ionizer (model 041-1), the electrodes next to the filament are at filament potential or even at the much more positive potential of the grid itself. Part of the emitted electrons is thus drawn towards these electrodes and is accordingly lost for ionization. From the solid angle under which the cage and the other electrodes are seen from the filament, it is estimated that up to 80% of the emitted electrons may be lost.

Second, it is only by the extractor potential that the ion paths in the INR can be controlled. This may be sufficient as long as charge effects within the INR play no significant role. Increased charge densities, however, create potential pits that trap ions if no compensating field can be applied.

Third, the maximum efficiency of the commercial ionizer is reached when the extractor potential is tuned to its minimum voltage (−18 V with regard to the cage). Extending the voltage range for the extractor would improve the efficiency. However, the resulting increase in the electric field within the comparatively long INR may broaden the distribution of the ion flight time in the QMA and may thus reduce the detector time resolution.

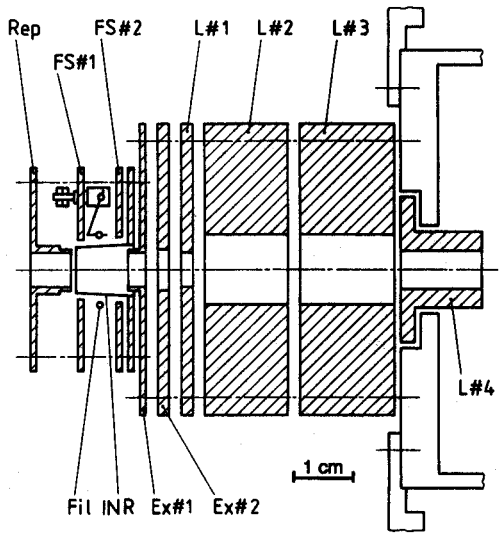

FIG. 2. Design of the ionizer. Rep=repeller electrode, FS=filament shield, INR=cage made of Ta wire enclosing the ionization region, Fil=electron emitting Ta filament surrounding the cage, Ex=extractor electrode, L=lens electrode. All the electrodes are electrically isolated from each other by ceramic spacers or sapphire balls. Their potentials are individually controlled.

We developed a design that suppresses these three disadvantages. The design is inspired by calculations of the electric potential on the points of a spatial grid[15] and on ion trajectory simulations,[16] and is based on the following concepts.

The first idea is to better utilize the electrons emitted from the filament. To this end we place on the sides of the filament two electrodes (FS 1 and FS 2 in Fig. 2), the potential of which can be set so that electrons are repelled. Almost all of the emitted electrons are thus accelerated towards the INR.

The second consideration is the following: It is well known that ion optics (like classical optics) cannot compress the phase-space volume occupied by the particles in a beam. The QMA establishes strict phase-space margins if the injected ions are to follow stable trajectories (see discussion in Sec. II). The ion optics can only serve to adapt as well as possible the phase-space volume of the ion source to the shape of the phase-space volume accepted by the QMA. This adaptation can essentially be accomplished by a single lens. Therefore we have to construct the INR as a source that provides ions which are already concentrated within a small phase-space volume. A perfect ion source would create all ions at the same potential and focus them into a single point. Then all ions could be refocused at the QMA entrance under an angle small enough to allow stable trajectories and thus 100% transmission could be achieved. Our approach to maximize the transmission is to introduce more control over the ion paths *within* the INR.

The space charge due to the electrons in the INR creates

a potential well (with the minimum on the beam axis) in which the ions oscillate about the INR axis while they are extracted. Initially the momentum of the ions forms a large angle with the INR axis.[17] The cage is given a conical shape so that reflections from the walls of the potential well reduce the angle between ion trajectory and beam axis. For a homogenous charge distribution the conical cage also leads to a potential gradient in the direction of the beam axis.[18] As this gradient should not be too large, the full angle of the cone was chosen to be 9°.[19]

In order to improve extraction, a repeller (Rep in Fig. 2) is mounted opposite to the extractor. It pushes ions back from the beam entrance of the INR, thereby supporting the action of the extractor, which pulls the ions towards the exit. Both repeller and extractor together control the longitudinal field inside the INR. To obtain the same velocity spread in the ion beam as in conventional designs, this field can be chosen stronger because the region within which ions are created is shorter, as we will see in Sec. IV C.

As the aperture of extractor 1 extends almost over the whole diameter of the INR, the electric field of the next electrode (which has to be more negative than extractor 1) extends into the INR and controls the extracting field near the INR axis. It is for this reason that this electrode is labeled extractor 2. However, it also acts as a first focusing element.

Power supplies from the former Extranuclear Company, Inc., are used as ionizer power supply and QMA supplies. Extractor 1 is connected to an output that can be set between -100 and $+50$ V off the cage potential, leaving no restrictions to the maximization of efficiency. The additional voltages needed for two independent filament shield electrodes, the repeller, and two additional lens electrodes are provided by separate voltage dividers of an external -1 kV supply. The filament shields require an additional transistor circuit which provides a low output impedance, because an incoming electron current of several milliamperes should not change the selected potential.

A feature not improved in our design is the limitation of the supply for the electron bombardment energy to about 100 eV. As the maximum ionization efficiency for He is obtained at 110 eV and the potential on the axis of the INR is some 20–30 V more negative than the cage potential, the ionizer in fact operates some 30–40 eV below the optimum electron energy for He ionization. An increase of the electron energy would also reduce the space-charge effects in the INR. The additional improvement due to a supply with a larger voltage range for the cage could increase the efficiency by a factor of 2 at most.

We would like to emphasize that the improvement of the ionizer is not restricted to the ionization of He. It can also be used for a more efficient detection of any type of atom or molecule. If a different species is to be ionized, the necessary changes concern the electron energy (to achieve optimum ionization efficiency) and an increase in QMA resolution ($m/\Delta m > 10$). For example, a reduction of electron energy results in more severe space-charge problems in the INR, while an increase in resolution reduces the maximum allowed ion velocity and further restricts the QMA injection conditions. Both maximum allowed velocity and injection conditions are determined by the required mass resolution and scale as $\sqrt{\Delta m/m}$.[12]

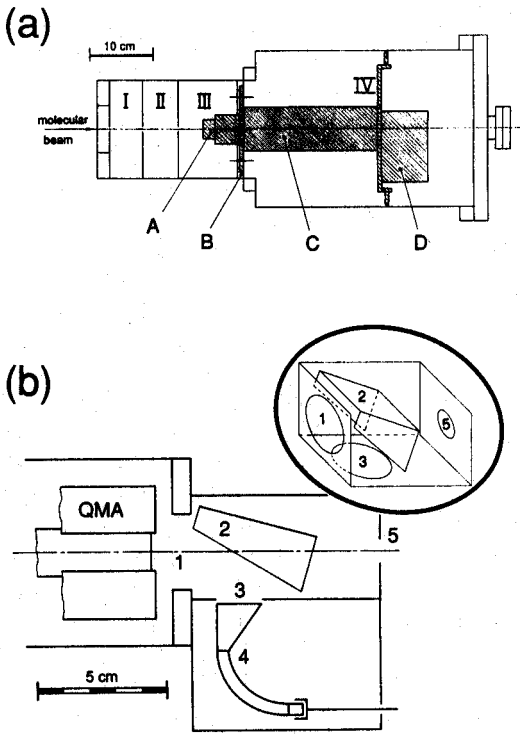

FIG. 3. (a) Schematic setup of the complete detector device with four differentially pumped UHV chambers. The letters represent: A—ionizer, B—tight fitting of the removable detector assembly (shaded part) to the UHV chamber III, C—QMA, and D—channeltron box. (b) Deflector design: The main scheme shows a section through the channeltron box, the inset on the right hand side gives a three-dimensional aspect. The numbers represent: 1—QMA exit, 2—deflector, 3—channeltron entrance, 4—channeltron, and 5—exit of neutral beam.

B. Background reduction

In order to achieve a large signal-to-noise ratio an extremely low background pressure is required in the INR. Therefore the neutral beam has to pass freely through the detector without hitting any obstacle, so that no source of diffuse He is created close to the INR. The detector unit shown in Fig. 3(a) consists of four differentially pumped UHV chambers. The INR is placed in chamber III, which is connected to the scattering experiment via the differentially pumped chambers I and II. These two pumping stages are particularly important when a low intensity He signal is detected, while the bulk of the He beam scattered from the sample under investigation (e.g., specularly reflected atoms) is not directed into the detector line but gives rise to a substantial He partial pressure in the sample chamber.

After having passed the INR the directional neutral beam enters chamber IV, where it is randomized by wall collisions. Chamber IV is differentially pumped, so that no large back flow into chamber III occurs which would result in an increased He background pressure in the INR. The only opening between chambers III and IV is the QMA entrance, a tube of 6 mm inner diameter and 13 mm in length, which is labeled L 4 in Fig. 2.

It is known already from the early experiments with QMAs that their linear geometry (in contrast, for example, to mass separation in a magnetic sector field) leads to a significant background counting rate by photons[2] and slow metastable neutrals that are created in the INR. In order to reduce this background, the channeltron has to be "out of sight" of the INR. Different geometries have been proposed.[20] We chose the geometry sketched in Fig. 1 in which the entrance plane of the channeltron is parallel to the beam axis. The channeltron entrance potential of −2.5 kV is strongly attractive for the positive ions. Ion trajectory calculations, however, indicate that only a small part of the broad ion distribution leaving the QMA (see Sec. II) will actually hit the channeltron entrance. The chosen geometry is favorable only if a deflector plate [Fig. 3(b)] is introduced. It is placed outside the trajectories of the neutrals, but its electric field bends the diverging trajectories of the ions towards the channeltron entrance. The experimental maximum of detection efficiency is obtained for deflector potentials between +500 V and +600 V if the channeltron entrance is at −2.5 kV. The efficiency increases by a factor of 20 compared to a grounded deflector.

IV. EXPERIMENT AND DISCUSSION

In this section we present measurements of the two essential properties of the detector: efficiency and time resolution. These two properties could not be measured with the same setup. Instead, two different types of molecular beams are needed, because an *a priori* well characterized molecular flux distribution is provided best by an effusive beam, while a highly monoenergetic velocity distribution, which is necessary to determine the time resolution, is generated best by a supersonic nozzle beam. Thus we can not discuss in full detail the correlation between efficiency and time resolution.

First of all, we will briefly introduce the adjustment procedure for the various ionizer potentials, as this is essential to obtain optimum performance.

A. Efficiency maximization

For the adjustment procedure we assume that the QMA has already been properly adjusted and the channeltron is set to about −2.5 kV.

The procedure of maximization of efficiency begins by setting all lens voltages to ground potential. The cage potential[21] is set between 40 and 60 V for a He beam (see maximum kinetic energy allowed by the QMA in Sec. II). The filament potential is set to −100 V with respect to the cage voltage. The deflector potential with respect to the ground is +550 V. The filament shields are set 10–40 V more negative than the filament, with FS 1 more negative than FS 2. Extractor 1 is set 5–10 V more negative and the repeller 5–10 V more positive than the cage voltage. The emission current is set to the desired value (0.01–15 mA).[22] Next the voltage of extractor 2 is lowered beginning from the voltage of extractor 1 until the counting rate exhibits a maximum. Finally, lens 2 is tuned to increase the counting rate to an even higher maximum. At this point a significant counting rate will be reached and several fine tuning cycles can follow. Most reasonably, each cycle begins with the potentials determining the electron paths, then the ion paths in the INR are readjusted. The procedure continues step by step towards the QMA entrance and finishes with the deflector plate.

Extractor 1 is usually set about 10 V negative with respect to the cage and extractor 2 another 10–50 V more negative. When the voltage of extractor 1 is increased to approach the cage potential and becomes even more positive, the counting rate can exhibit a sharp maximum. In this situation TOF measurements usually show a tail of delayed ions. Due to the increased potential of extractor 1, the effective exit aperture of the INR which is formed by the electrostatic potential is obviously narrowed. The INR forms an ion cage from which ions can escape only when they pass through extractor 1 close to the beam axis. In our interpretation the observed maximum is due to a reduction of the phase space occupied by the ions, i.e., it is due to the improvement of the ion source quality. Whenever maximum time resolution is dispensable, this setting is favorable.

While the control of the ionization region requires the adjustment of five potentials, there is usually no need to adjust more than one of the lens electrodes, for example, lens 2. The other lenses can be kept at ground potential without essential loss in efficiency.

In order to obtain an estimate of η, the number of times an electron traverses the INR, the filament shield voltages are chosen slightly more positive or somewhat more negative than the cathode. In the first case emitted electrons are accelerated in all directions and not all of them will traverse the ionization region. When reaching the opposite side of the INR, the probability of traversing the INR once more is very small. However, for filament shields that are a few volts more negative than the filament, all emitted electrons are accelerated towards the INR and when emerging on the opposite side, they are reaccelerated towards the INR. The ratio of the counting rates between these two situations was measured to be 3. This value can be interpreted as an upper limit for the number of times an emitted electron traverses the INR. The result can be compared to the one obtained for a simple model which assumes that the electron transmission of the cage equals its optical transmission.[23] In fact, for the optical transmission of the mesh of 85%, a mean number of 3 passes is obtained. As this model neglects other aspects, we will assume in the following that the true value lies between 2 and 3.

B. Experimental detection efficiency

The detection efficiency is defined as the number of ions counted by the channeltron divided by the number of He atoms passing through the ionization region. Figure 4(a) shows the setup used to determine the detection efficiency for He. A room-temperature effusive beam passes through a diaphragm and is detected by the ionization detector. The solid angle of the diaphragm as seen from the source is 6.8×10^{-6} sr and all molecules pass through a cylindrical volume of 1.5 mm in diameter in the center of the INR. For estimates of ionization efficiency, however, the effective beam diameter of 1 mm has to be used because the intensity of the real beam decreases with increasing distance from the axis, which is due to the finite diameter of the source aperture. The effusive source is calibrated by measuring the time

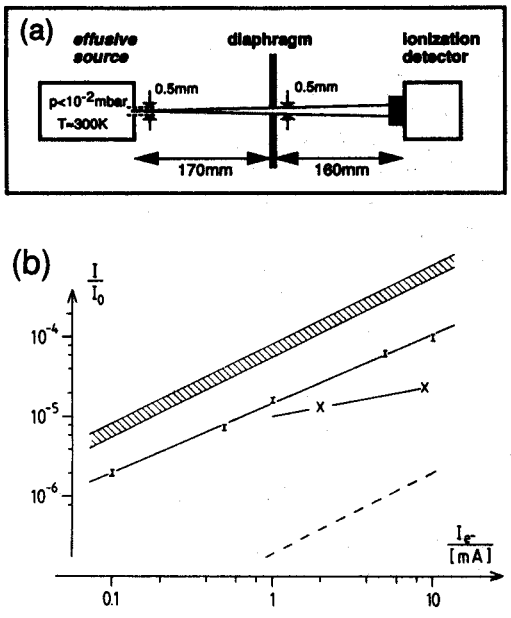

FIG. 4. (a) Geometry of the setup used to measure absolute detection efficiencies. (b) Efficiencies for He detection as a function of electron emission current in double-logarithmic presentation. The experimental data (with error bars) obtained for a 300 K effusive beam of 1.5 mm diameter are shown. The crosses mark the results at maximum efficiency when tails in time-of-flight measurements have been suppressed. The shaded area represents the range of the theoretically estimated ionization efficiencies k [from Eq. (1)]. The dashed line indicates the efficiency of the commercial ionizer (see text).

within which a gas reservoir of known volume V, and initial pressure p_i supplies the effusive cell. When the pressure in the reservoir has dropped to a value p_f after the time Δt and the flux from the cell was held constant during this time, the flux of molecules from the effusive source has obviously been

$$\dot{N}=\frac{V(p_i-p_f)}{k_BT\Delta t}. \tag{2}$$

All parameters in this formula except the pressure can be determined with an accuracy of a few percent. The absolute accuracy of the flux thus equals the accuracy for a calibrated Pirani manometer (corrected for He) which is $\pm 10\%$ according to the supplier.[24] In view of the cosine distribution of the effusive source, the flux in forward direction (i.e., perpendicular to the aperture of the effusive source) into a solid angle $\Delta\Omega \ll 1$ is $\dot{n}=\dot{N}\Delta\Omega/\pi$.

In Fig. 4(b) we plot efficiencies as a function of electron emission. The measured detection efficiencies for the detector presented here are marked by error bars, which indicate the absolute accuracy. For each measurement the detector efficiency was maximized as described in Sec. IV A. At emission currents above 1 mA, tails appear in time-of-flight measurements, which reduces the effective time resolution of detection. The crosses in Fig. 4(b) mark the maximum efficiencies when the proper detector time resolution is restored. The ionization efficiency k, which is only one factor in the detection efficiency (see Fig. 1) is estimated from Eq. (1) and represented here by the shaded region. The height of the region results from the fact that the exact value for η in Eq. (1) is not known ($2 \leqslant \eta \leqslant 3$). The detection efficiency of the commercial detector (Extranuclear model 041-1, with QMA model 4-324-9 and channeltron)[4] is indicated by the dashed line.

The comparison of the different detection efficiencies in the most frequently used range of the emission current (1–10 mA) shows the following: The measured detector efficiency yields more than 10% of the theoretical efficiency of the ionizer alone (shaded region). The detector is improved with respect to the standard commercial system by a factor of 50–75 at 1 mA electron emission current, where the first figure holds for the case of suppressed TOF tails. At 10 mA emission the improvement is, respectively, 10 and 50. The efficiencies given in Fig. 4(b) are directly applicable to a monochromatic beam of $v=1260$ m/s, which corresponds to a supersonic He beam at 150 K nozzle temperature.

C. Experimental time resolution

To our knowledge detector time resolutions near 1 μs have not been measured directly so far. This parameter is generally obtained as the residual error in time-of-flight measurements after the contributions from beam chopping and energy spread of the molecular beam have been subtracted. Here, we present a measurement which is dominated by the excellent time resolution of the detector.

The FWHM of the measured time-of-flight spectra does not depend strongly on the detailed electrode voltage settings. However, if only the efficiency is maximized without paying attention to time resolution, tails emerge at electron emissions above 0.5 mA. The tails have maximum intensities of some 10% of the peak height and extend over approximately 20 μs.[25] Tails, however, have to be suppressed completely for time-of-flight measurements. In general, this problem does not arise for small emission currents. At higher currents, however, the space charge in the INR becomes important and a significant amount of ions may become trapped in the INR for a few microseconds before they pass through the exit of the INR.

In the following measurement of the detector time resolution we are mainly interested in determining the effective ionization length which corresponds to the width of the formed electron beam. No detailed investigation on ion trapping and the formation of tails is undertaken.

The high-vacuum setup used for the experiment [see Fig. 5(a)] is described in detail elsewhere.[26] In short, it consists of a high-pressure He nozzle source which creates a highly monochromatic room-temperature He beam. Pulses of 0.7 μs FWHM are generated by a tiny chopper[26] which is positioned at a distance of 150 mm from the INR of the detector. The pulse dispersion on this flight path is $\Delta\tau=0.7$ μs FWHM. In Fig. 5(b) and 5(c) we show the measured time response of the detector in this setup at 5 mA electron emission current with repulsive filament shields. No significant tails are visible. In Fig. 5(b) the measured pulse width of 1.8 μs FWHM is dominated by the detector resolution. This becomes apparent from Fig. 5(c), where the width of the time response is narrowed down to 1.4 μs by changing one filament shield potential.

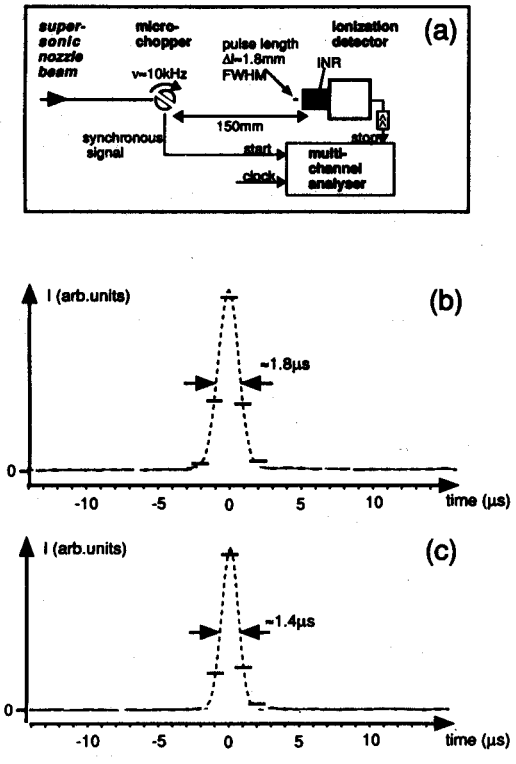

FIG. 5. Time response of the ionization detector to a short thermal energy He pulse. (a) Experimental setup employed for the measurement. The channel width of the analyzer is 1 μs. (b) and (c) show measurements of the detector time response. The short horizontal lines represent the counting rate accumulated in the multichannel analyzer. The dashed lines are Gaussians that reproduce the measurements when being integrated over the channel width of the analyzer. The arrows mark the full width at half maximum of the Gaussian. Measurement (b) was recorded at 5 mA electron emission with repulsive filament shields (FS 1: -40 V, FS 2: -9 V with respect to the INR). (c) was recorded under the same conditions as (b) except that the potential of filament shield 2 was lowered by 6 V (FS 2: -15 V).

At thermal beam energies, the length of the INR is the most adequate quantity to describe the time resolution of the ionizer, because supplementary contributions like the ion flight time dispersion and the electronic broadening are smaller than 0.5 μs. With the He beam velocity of $v=1800$ m/s the result from Fig. 5(b) leads to an effective length of the INR between 3.2 and 2.7 mm FWHM, where the latter value is obtained after subtraction of the estimated contribution due to the finite pulse length. We can conclude that the width of the ionizing radial electron beam is substantially smaller than the spacing between the filament shields (6 mm), which demonstrates that the electron beam is not diverging but narrowed down due to the directing effects of the repulsive filament shields. The effective length of the INR of the commercial ionizer was formerly estimated from time-of-flight measurements for He to be at least 5 mm in the emission current range between 1 and 5 mA.[4] Taking into account that the ionization efficiency of the ionizer presented here has been significantly increased at the same time, the detector appears particularly suitable for time-resolved He detection.

V. CONCLUSION

We have developed and characterized an electron-impact ionization detector for energy resolved He surface scattering devices.

The development is based on potential calculations and on ion path simulations and essentially concerns improvements of the ionizer unit. The electrons emitted from the filament are practically all accelerated towards the ionization region, which results in a high efficiency already at low emission currents (<1 mA). The ion extraction from the ionization region and thus the quality of the ion beam can be controlled in detail to improve the transmission through the mass analyzer. A deflector improves the collection of ions by the channeltron.

The ionizer design demonstrates that a comparatively large charge density can be combined with a clearly structured and still easily operable electrode system to yield an excellent time resolution together with a detection efficiency of 10^{-4} at 10 mA. The efficiency thus exceeds 10% of the estimated maximum ionization efficiency. For atom beam time-of-flight application even small tails in the flight time distribution have to be suppressed and the efficiency reduces to 2×10^{-5} at 10 mA. Under these conditions the efficiency increases substantially slower than proportional to the electron emission. The results indicate that a suppression of tails is possible only at the expense of detection efficiency. The measured efficiency is one to two orders of magnitude larger than the one of a commercial ionizer under identical operation conditions.

Although the design was developed for the detection of thermal energy He beams, the ionizer can also be employed for a more efficient ionization detection of any type of atom or molecule.

APPENDIX: CHARGE DENSITY AND POTENTIAL IN THE IONIZATION REGION

In this part we derive estimates for the charge density and the resulting potentials in the INR. No exact solution can be obtained for the region close to the axis.

Following the arguments in Ref. 23 we estimate the mean charge density in the INR in the following way: At an electron energy of 100 eV the time an electron needs to traverse the cage (8 mm diameter) is 1.3 ns. If we assume that on the average an electron crosses the cage $\eta=3$ times, each emitted electron spends 4 ns in the cage. For a given emission current of 2 mA there are at any time 5×10^{7} electrons in the cage. This corresponds to a mean charge density of $\bar{\rho}=-5.3\times10^{-5}$ C/m^3 for an INR of 3 mm length and 8 mm diameter.

Assuming a homogeneous charge distribution in a cylindrical geometry the electric potential has a parabolic shape:

$$V(r)=V_{\text{axis}}+\frac{\bar{\rho}}{4\epsilon_0}r^2, \tag{A1}$$

where V_{axis} is the potential on the axis of the INR, r the distance from this axis, and ϵ_0 the free space permittivity. For the above parameters the potential difference between cage and axis becomes 24 V, the potential at $r=2$ mm from the

axis is 6 V with respect to the axis. For ions created more than 2 mm away from the axis, the radial field is already larger than the longitudinal (extracting) field. This results in an oscillatory motion of the ions in the INR during extraction.

The assumption of a homogenous charge distribution leads, however, to a very crude model. We can determine the charge density in the INR close to the cage by adapting a geometry in which we regard a small section of the grid as being flat. The electron flux density through the cage is

$$j=\frac{\eta I_{e^-}}{2\pi R l}, \tag{A2}$$

where R is the cage radius ($R=4$ mm) and l the length of the INR ($l=3$ mm). With $\rho = j/v_{e^-}$ and taking into account that the same amount of electrons passes through the grid in the opposite direction, the charge density of the electrons at the grid is $\rho_{\text{grid}}=-2.6\times10^{-5}$ C/m^3, which is exactly half of the mean charge density in the INR: $\rho_{\text{grid}}=\bar{\rho}/2$. It follows that the charge density near the axis must be much larger than $\bar{\rho}$. Thus the curvature of the potential near the axis is larger than given by Eq. (A1) and the potential difference between the axis and a position 2 mm from the axis thus exceeds 6 V. In the nonrealistic case of a perfect cylindrical symmetry where all electrons pass *exactly* through the axis, the infinite charge density on the axis would result in a potential that equals the potential of the emitting cathode (i.e., about 100 V more negative than the cage). A realistic estimate of the potential depends very sensitively on the details of the electron trajectories near the axis.

If the shape of the cage is not cylindrical but conical with a full angle of 9° (see Fig. 2), the diameter of the cage varies by $\Delta d=0.5$ mm over the length $l=3$ mm of the INR. According to Eq. (A1) the potential of the homogeneous charge distribution drops by about $\Delta V/V=2\times\Delta R/R$ in the direction of the increasing cage diameter. With the same parameters as used above, a longitudinal field of 6 V/3 mm is obtained. The conical shape of the cage thus promotes the extraction of the ions.

[1] He detectors for different applications are the Pirani gauge, x-ray ionization, and detection of metastable atoms excited by electron bombardment [K. M. Martini, W. Franzen, and M. El-Batanouny, Rev. Sci. Instrum. **58**, 1027 (1987)], and the spinning rotor gauge [K. Kern, B. Lindenau, R. David, and G. Comsa, Rev. Sci. Instrum. **57**, 277 (1986).].

[2] H. G. Bennewitz and R. Wedemeyer, Z. Phys. **172**, 1 (1963).

[3] G. O. Brink, Rev. Sci. Instrum. **37**, 857 (1966).

[4] R. David, K. Kern, P. Zeppenfeld, and G. Comsa, Rev. Sci. Instrum. **57**, 277 (1986).

[5] J. P. Toennies, J. Vac. Sci. Technol. A **2**, 1055 (1984); K. Kern and G. Comsa, Adv. Chem. Phys. LXXVI p. 211 ff. (1989), and references therein.

[6] R. David, K. Kern, P. Zeppenfeld, and G. Comsa, Rev. Sci. Instrum. **57**, 2771 (1986); D.-M. Smilgies and J. P. Toennies, Rev. Sci. Instrum. **59**, 2185 (1988); K. Kuhnke, Ph.D. thesis, Berichte des Forschungszentrums Jülich, Jül-2490, 1991.

[7] Or, equivalently, the length over which the average electron trajectory intersects with the beam of neutrals.

[8] The emission current is defined as the electron current leaving the filament and ending up on any part of the device except on the filament itself.

[9] H. S. W. Massey, E. H. S. Burhop, and H. B. Gilbody, *Electron and Ionic Impact Phenomena*, 2nd ed. (Oxford University, New York, 1969), Vol. I, p. 128.

[10] The formula on page 153 in W. Paul, H. P. Reinhard, and U. von Zahn, Z. Phys. **152** (1958), would give a limit of 150 eV; the formula, however, is valid for resolutions $m/\Delta m$ near 100 rather than for the resolution of 10 that we require here. An additional increase of residence time in the QMA of 60% leads to a separation that is experimentally satisfactory.

[11] For model No. 4-324-9 with high-Q head model 11 from the former Extranuclear Laboratories, Inc.

[12] W. Paul, H. P. Reinhard, and U. von Zahn, Z. Phys. **152**, 143 (1958).

[13] The QMA electrode potentials oscillate with an ac amplitude of 500 V. An ion leaving the QMA experiences the ground potential outside the QMA either as repulsive or attractive. Ions leaving the QMA close enough to an electrode can thus be reflected from the exit, can be slowed down or they can gain a significant additional kinetic energy.

[14] The ions oscillate in the QMA with amplitudes of several millimeters at frequencies above 2.2 MHz. Thus the ion trajectory can be at a significant angle with respect to the QMA axis at the instant when the ion leaves the QMA.

[15] See, for example, G. Shortly, R. Weller, P. Darby, and E. H. Gamble, J. Appl. Phys. **18**, 119 (1947); H. Wollnik, in A. Septier, ed., *Focussing of Charged Particles* (Academic, New York, 1967), Vol. 1/2.

[16] For example, O. Klemperer, *Electron Optics* (Cambridge University, New York, 1971).

[17] The gradient along the axis is about 2 V/mm, while the potential 1 mm from the axis is more than 1.5 V higher than on the axis (see Appendix).

[18] See R. Weiss, Rev. Sci. Instrum. **32**, 397 (1961); the effect is also described in the Appendix.

[19] From the simplified geometry on which Eq. (A1) is based, one obtains, for example, a decrease of 5.7 V over the ionization length of 3 mm.

[20] F. Nakao, Rev. Sci. Instrum. **46**, 1489 (1975), and references therein.

[21] The grid potential is often incorrectly called "ion energy" although these two potentials differ by the potential bending resulting from space charges in the INR.

[22] We have operated the filament, which is simply a ring of 0.1 mm Ta wire, at 15 mA for several days without problems. In long term operation at 2–5 mA emission the filament will work for more than one year.

[23] C. Félix, Diploma thesis EPF Lausanne Switzerland, 1991.

[24] Leybold-Heraeus, Grundlagen der Vakuumtechnik, Berechnungen und Tabellen, No. 70/A0 15.1.1. der Werksgruppe Vakuumseriengeräte.

[25] Even for detector settings in which simply the total counting rate was maximized, the tail never provided the dominating contribution to the peak height in time-of-flight spectra, although the integrated intensity in the tail may dominate the total counting rate.

[26] K. Kuhnke, K. Kern, R. David, B. Lindenau, and G. Comsa, Rev. Sci. Instrum. **65**, 653 (1994).